

# Unusual energy spectra of matrix product states

J. Maxwell Silvester<sup>1</sup>, Giuseppe Carleo<sup>2</sup>, and Steven R. White<sup>1</sup>

<sup>1</sup>*Department of Physics and Astronomy, University of California, Irvine, California 92667, USA and*  
<sup>2</sup>*Institute of Physics, École Polytechnique Fédérale de Lausanne (EPFL), CH-1015 Lausanne, Switzerland*  
 (Dated: August 27, 2024)

In the simulation of ground states of strongly-correlated quantum systems, the decomposition of an approximate solution into the exact eigenstates of the Hamiltonian—the energy spectrum of the state—determines crucial aspects of the simulation’s performance. For example, in approaches based on imaginary-time evolution, the spectrum falls off exponentially with the energy, ensuring rapid convergence. Here we consider the energy spectra of approximate matrix product state (MPS) ground states, such as those obtained with the density matrix renormalization group (DMRG). Despite the high accuracy of these states, contributions to the spectra are roughly constant out to surprisingly high energy, with an increase in bond dimension reducing the amplitude but not the extent of these high-energy tails. The unusual spectra, which appear to be a general feature of compressed wavefunctions, have a strong effect on sampling-based methods, yielding large fluctuations. For example, estimating the energy variance using sampling performs much more poorly than one might expect. Bounding the most extreme samples makes the variance estimate much less noisy but introduces a strong bias. However, we find that this biased variance estimator is an excellent surrogate for the variance when extrapolating the ground-state energy, and this approach outperforms competing extrapolation methods in both accuracy and computational cost.

Numerical simulations of a variety of sorts have become essential for the study of quantum many-body systems. Given an approximate ground state,  $|\psi\rangle$ , we consider its decomposition into exact energy eigenstates, i.e., its energy spectrum,

$$|\psi\rangle = \sum_n c_n |n\rangle, \quad (1)$$

where  $\{|n\rangle\}$  are the eigenstates of the Hamiltonian with corresponding energies  $\{E_n\}$ . For a number of numerical approaches based on imaginary-time evolution, e.g. quantum Monte Carlo, the coefficients  $c_n^2$  fall off exponentially with the gap  $E_n - E_0$ , where  $E_0$  is the ground-state energy [1, 2]. This exponential fall-off provides strong guarantees on convergence rates, particularly where there are no near-degeneracies. Because the density matrix renormalization group (DMRG) can achieve very accurate ground-state energies, one might assume that the high-energy coefficients of the corresponding matrix product state (MPS) would also fall off rapidly as the energy gap increases [3–8]. Since producing the spectrum of a DMRG state requires a full diagonalization of the Hamiltonian, it is only available on small test systems. Surprisingly, we find that the high-energy coefficients do not decrease exponentially with the gap. In fact, for a substantial energy range they do not decrease much at all.

In Fig. 1 we show spectra for a spin  $S = 1/2$  Heisenberg model on a  $4 \times 4$  square lattice cluster. A description of all the models we consider can be found in the supplementary materials (SM)[9]. We compare DMRG results to those from an exact imaginary-time evolution (ITE) starting with a Néel state. The imaginary-time duration,  $\tau$ , is chosen to make the two states have approximately the same energy. Note that we choose fully periodic boundary conditions, for which DMRG requires

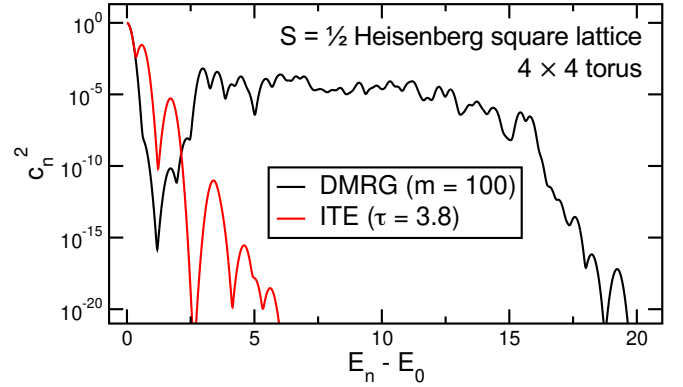


FIG. 1. Energy spectra of approximate ground states from DMRG and imaginary-time evolution (ITE) for a small cluster with fully periodic boundary conditions, broadened by Gaussians with width 0.1. The states are matched to have the same energy, with  $E - E_0 = 0.016$ , but the energy variance  $\sigma_H^2$  is much larger for DMRG, 0.119 versus 0.0092.

larger bond dimension to achieve accurate results, in order to emulate a DMRG run on a larger system while still being able to fully diagonalize the Hamiltonian. A clear exponential tail is seen for the ITE spectrum, as expected. In contrast, the DMRG spectrum has very little weight in the first few excited states and a tail that is roughly constant out to surprisingly high energies.

In this Letter, we show that these high-energy contributions to DMRG wavefunctions appear quite generally across different lattice models and geometries, and explore important implications of such spectra for sampling-based methods.

*Unusual spectra*—Such unusual energy spectra are due to the compression of the state into an MPS, rather than some aspect of the DMRG energy optimization. This is

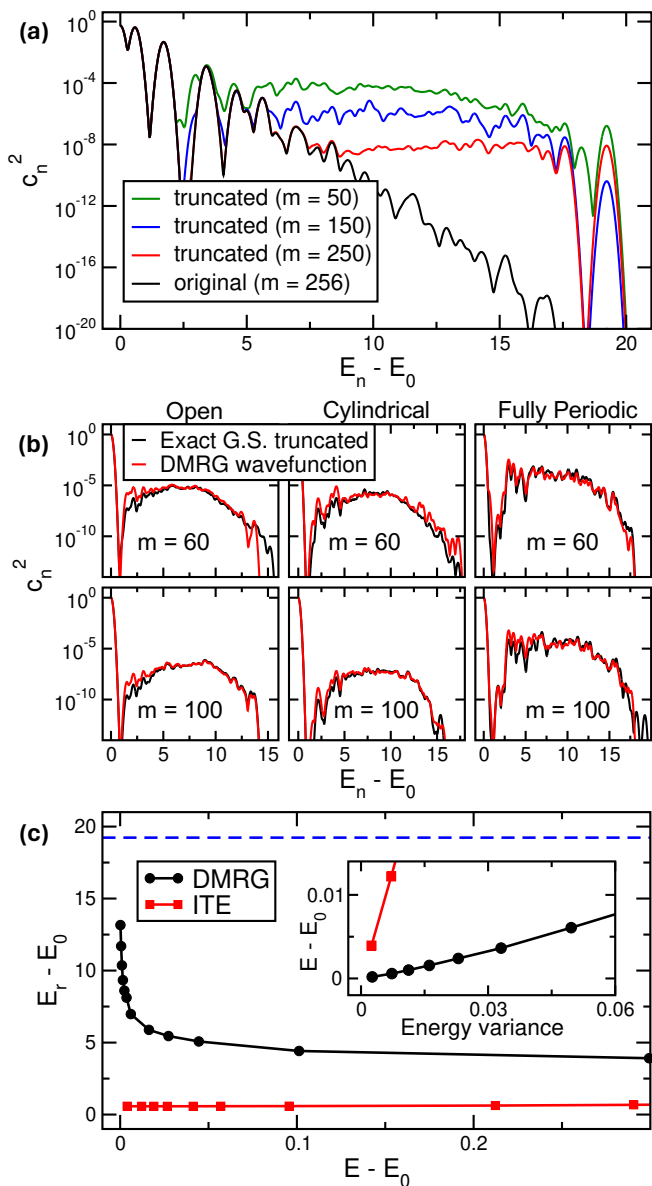


FIG. 2. Results for a  $4 \times 4$ ,  $S = 1/2$  Heisenberg square lattice with various boundary conditions. (a) For fully-periodic boundary conditions (PBC), the effect of truncating an ITE state ( $\tau = 1$ ) when it is represented as an MPS. Energy spectra obtained via exact diagonalization (ED) and broadened with Gaussians. (b) Comparing the states obtained via truncating the exact ground states to bond dimension  $m$  vs the states obtained via running DMRG at the same bond dimension. Again results obtained via ED and broadened. (c) For PBC, the energy of the residue vs the energy error of a solutions from both DMRG and ITE. The blue dashed line indicates the difference between the maximum and minimum eigenenergies of the system. On the inset, the energy error of the state vs the energy variance. Points on the main plot and inset indicate distinct bond dimension or imaginary-time  $s$  for the DMRG and ITE states, respectively.

shown in Fig. 2(a), where we compress an ITE state into an MPS. The spectrum flattens at an energy gap deter-

mined by the bond dimension,  $m$ . Note that for this small cluster, the maximum bond dimension for any state to be represented exactly is  $m = 256$ , the Hilbert space dimension of half the system. It is remarkably that the flat tail is apparent even with a truncation to  $m = 250$ . While some details of the results of Fig. 2(a) are specific to the fully periodic boundaries, the qualitative behavior is independent of boundary conditions. This is illustrated in Fig. 2(b), where we compare DMRG spectra to spectra obtained from truncating the exact ground-state to the same bond dimension as the corresponding DMRG state. Regardless of bond dimension or boundary conditions, the spectra show similar qualitative features, extending to high energy. Moreover, in each case the DMRG spectrum matches closely the spectrum from truncation of the exact solution, confirming that indeed the spectra are a result of the compressed MPS representation of the wavefunction.

It is also interesting to consider the average energy of a DMRG state when the exact ground state is projected out, i.e., the energy of the excited part of the solution. Thus, we decompose the approximate ground state as

$$|\psi\rangle = \sum_n c_n |n\rangle = \cos\theta |0\rangle + \sin\theta |r\rangle, \quad (2)$$

where the *residue*,  $|r\rangle$ , is normalized. In Fig. 2(c) we show the average energy of the residue, i.e.,  $E_r = \langle r|\hat{H}|r\rangle$ , versus energy error as we vary the bond dimension in a DMRG calculation. Remarkably,  $E_r$  increases sharply as the bond dimension is increased, eventually reaching about  $2/3$  of the total energy bandwidth (dashed blue line). Of course, this increase in the residue's energy is more than compensated for by a decrease in  $\theta$ , so that the  $E - E_0$  still approaches zero. In contrast, for the ITE state, with increasing  $\tau$ ,  $E_r$  simply approaches  $E_1 = \langle 1|\hat{H}|1\rangle$ , the energy of the first excited state.

The striking dissimilarity between the residues of the DMRG and ITE states provides a way to probe the energy spectra of larger systems, where exact diagonalization is unavailable. Note that for the special case when  $|r\rangle = |1\rangle$ , i.e., when all of the error in the approximate ground-state is in the first excited state, the quantity

$$\tilde{v} = (E - E_0)^2 \cos^2\theta + (E - E_1)^2 \sin^2\theta. \quad (3)$$

is equal to the wavefunction's energy variance,  $\sigma_{\hat{H}}^2 = \langle \psi | (\hat{H} - E)^2 | \psi \rangle$ . Importantly, calculating  $\tilde{v}$  requires only quantities that can be easily estimated within DMRG, such as the lowest energy gap. The ratio  $\sigma_{\hat{H}}^2 / \tilde{v}$  serves as a measure of the high-energy contributions to the wavefunction. Specifically, for ITE states, this ratio reduces to unity as the ground state is approached. In contrast, for DMRG wavefunctions this ratio steadily increases as the MPS converges, reaching values of  $10^2 - 10^4$  or higher. This prominent signal is seen across different geometries, boundary conditions, and models, as described in the SM [9], showing that high-energy residues are a quite-general feature of MPS solutions.

Why do MPS spectra have these high-energy tails? Suppose they did not; imagine instead that like an ITE state, an MPS state of low bond dimension was, to high accuracy, composed of a small number of excited states. The MPS representation of each of these excited states will have high bond dimension, since we do not consider them to be approximate. Then, in forming the low bond dimension DMRG state as a linear combination of the few large bond dimension states, we would need a precise cancellation of a huge number of parameters. This cancellation is reasonable only if the number of states we are combining is comparably large, therefore requiring that they extend to high energy. Note that this reasoning is not very specific to MPS states: not only would it apply to other tensor network states, but to any type of state that can be considered a general compression of the exponentially large space, e.g., a neural network state.

*Consequences for sampling*—To highlight the strong effect that MPS spectra can have on sampling-based methods, we now consider the specific task of calculating the energy variance of the state, first reviewing non-sampling approaches. Note that in the inset of Fig. 2(c), where the black and red dots represent successive DMRG sweeps or increasing  $\tau$ , respectively, the DMRG state has a much higher variance than the ITE state, for fixed energy error,  $E - E_0$ . While this discrepancy—a direct consequence of the high-energy tails—may make comparisons of different numerical methods based on energy variance misleading[10], the near-linear behavior shows that the variance may still be an ideal candidate for extrapolating the energy to the infinite bond dimension, zero variance limit. Unfortunately, computing the exact energy variance of a DMRG wavefunction is more expensive than a DMRG sweep by a factor of  $w$ , the bond dimension of the Hamiltonian expressed as a matrix product operator. For systems with long-range interactions or two-dimensional (2D) geometry we may have  $w \sim 30$  or greater.

Historically, it has instead been standard practice in DMRG calculations to perform extrapolations in the truncation error, i.e., the total probability of the states that are thrown away during sweeping to compress the state[5, 11, 12]. Not only do such extrapolations provide error bars, but non-linearity in the energy versus truncation error can also indicate that the initial wavefunction was far from the ground state and the system is not well converged. While the truncation error is calculated at almost zero computational cost during a DMRG sweep, it depends on details of the sweeping, and producing a truncation error usable for extrapolation requires care in the construction of the sweeping procedure. In cases with long-range interactions, truncation error extrapolations may be unreliable. Moreover, estimating the truncation error is unavailable in the single-site implementation of DMRG, which is cheaper than the two-site algorithm[13, 14].

More recently, the *two-site variance* has been introduced as a means to approximate the energy vari-

ance of the DMRG wavefunction at an affordable cost, enabling extrapolations when running single-site DMRG[15]. While this quantity is an accurate approximation of the variance for nearest-neighbor one-dimensional (1D) open chains, it can deviate strongly for 2D systems. However, its errors are systematic and the two-site variance vanishes when the state is an exact eigenstate. Thus, this quantity can be used to produce high-quality extrapolations. The cost of computing the two-site variance is similar to that of a DMRG sweep, roughly doubling run-time if the variance is calculated every sweep.

As another alternative to estimate the variance cheaply, we consider using sampling. Unlike in many quantum Monte Carlo algorithms, which construct a Markov chain with nonzero autocorrelation times, MPS states can be sampled with one perfectly independent sample per step. This so-called perfect sampling technique is the starting-point of both the minimally entangled typical thermal state algorithm and MPS-based variational Monte Carlo methods[16–19]. A sample is a product state  $|s\rangle$ , where the product is over states of each site, which is generated with probability  $P_s = |\langle\psi|s\rangle|^2$ . The product states form a complete basis,  $\mathcal{B}$ , so that we may rewrite the energy variance as

$$\sigma_{\hat{H}}^2 = \sum_{|s\rangle \in \mathcal{B}} \langle\psi|\hat{H} - E|s\rangle \langle s|\hat{H} - E|\psi\rangle, \quad (4)$$

where  $E = \langle\psi|\hat{H}|\psi\rangle$  is the expectation value of the energy. The *support*,  $\mathcal{S}$ , is the set of basis vectors for which  $P_s$  is nonzero. For states in  $\mathcal{S}$ , we define the *local energy*,  $E_s^L = \frac{\langle s|\hat{H}|\psi\rangle}{\langle s|\psi\rangle}$ ; outside  $\mathcal{S}$ , the local energy is undefined. Then, splitting the sum in Eq. (4) into two parts, we have

$$\sigma_{\hat{H}}^2 = \Delta_s + \sum_{|s\rangle \in \mathcal{S}} P_s |E_s^L - E|^2, \quad (5)$$

where the *local energy bias* is

$$\Delta_s = \sum_{|s\rangle \notin \mathcal{S}} \|\langle\psi|\hat{H}|s\rangle\|^2. \quad (6)$$

Note that, alternatively, an unbiased estimator can be obtained by inserting the identity operator next to  $(\hat{H} - E)^2$  in Eq. (4), instead of between the two copies of  $(\hat{H} - E)$ . In that case the samples with  $P_s = 0$  do not contribute to the variance. However, in the cases we have studied, the sampling bias  $\Delta_s$  is typically small, and it can be shown to rigorously vanish for exact eigenstates; usually, it can be ignored. We also find that the unbiased version of sampling is both more expensive and also prone to worse fluctuations, so we utilize the local energy sampling[9].

With  $N_s$  samples, the sampling estimate of the energy variance is

$$\sigma_{\hat{H}}^2 - \Delta_s \approx \frac{1}{N_s} \sum_{i=1}^K |E_i^L - E|^2. \quad (7)$$

The cost of selecting a product state,  $|s\rangle$ , in a perfect measurement, is  $\mathcal{O}(m^2d + md^2)$ , where  $m$  is the bond dimension of the MPS and  $d$  is the number of states on one site. Somewhat more expensive is a calculation of  $E_s^L$ , which scales as  $\mathcal{O}(m^2dw + md^2w^2)$ , where  $w$  is the bond dimension of the Hamiltonian MPO. This is a factor of the bond dimension  $m$  less expensive than a DMRG sweep, which scales as  $\mathcal{O}(m^3dw + m^2d^2w^2)$ . Estimating the variance via sampling can cost less than or be comparable to a sweep, provided that we take a modest number of samples, i.e.,  $N_s < m$ , where typically  $m \sim 1000 - 10000$ . In Fig. 3(a) we plot both the two-site and sampled variance of an approximate solution from DMRG, for a nearest-neighbor 2D Heisenberg cluster with periodic boundary conditions. With on the order of a thousand samples, our method provides a better variance estimate than the two-site variance, which is quite inaccurate due to the 2D geometry and periodic boundary conditions.

Despite its relative success in Fig. 3(a), the sampled variance is noisy, with large fluctuations even after hundreds of thousands of samples; near sample 200,000 is a large jump in the running average, due to a sample with a very large local energy deviation. We believe the large fluctuations we see in sampling the energy variance are closely tied to the unusual energy spectrum. In general, some error measure is a good candidate for extrapolation if it reduces smoothly and predictably to zero in the limit of large bond dimension. Because of these large fluctuations, the standard sampling of the variance does not in general produce good extrapolations. Even in cases such as Fig. 3(a) where the sampled variance is more accurate, the non-stochastic nature of the two-site variance makes it a better error measure for extrapolation.

To understand and potentially eliminate the noisiness, we investigate the sampling statistics in more detail. For small systems such as the one used for Fig. 3(a), it is possible to enumerate every sample and compute its local energy. Results from such an analysis are shown in Fig. 3(b) - (c). We see a dramatic difference in the local energy probability distributions. The DMRG distribution has samples with very small probability but substantial contributions to the variance. For example, consider the two samples near  $P_s \sim 10^{-8}$  in Fig. 3(b): these contributed  $\sim 10^{-4}$  to the variance each, so they must have  $|E_s^L - E|^2 \sim 10^4$ . Such extreme outliers for the DMRG state, as shown explicitly in Fig. 3(c), explain the sudden spikes in the running average.

*Biased variance extrapolation*—Given large fluctuations in the probability distributions, one is tempted to eliminate the outliers in some way. We consider bounding the local energy to within a symmetric interval of the exact energy,  $E$ , which is known from the DMRG sweep. Letting  $\epsilon = E_s^L - E$ , we define the piece-wise function

$$f(\epsilon) = \begin{cases} -\epsilon_{\max} & \text{if } \epsilon < -\epsilon_{\max} \\ \epsilon & \text{if } -\epsilon_{\max} \leq \epsilon \leq \epsilon_{\max} \\ \epsilon_{\max} & \text{if } \epsilon > \epsilon_{\max} \end{cases} \quad (8)$$

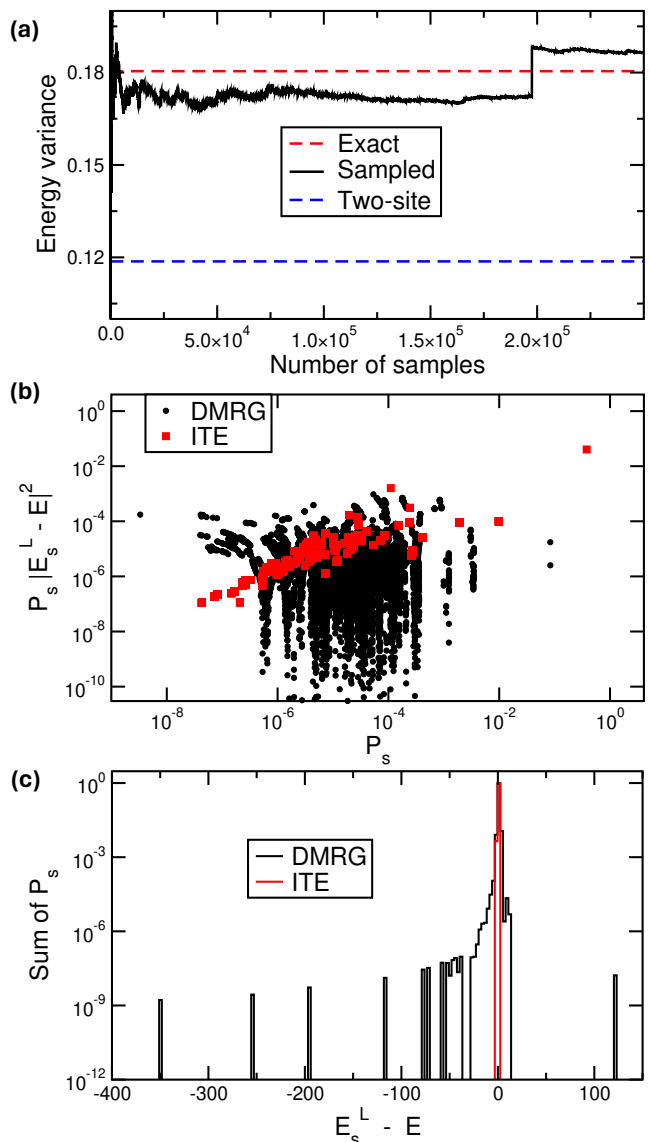


FIG. 3. For the same  $4 \times 4$  torus, (a) the running average of the sampled variance, the two-site variance, and the exact energy variance, all for the same DMRG state ( $m = 80$ ). (b) the probability distribution of local energies for approximate ground-state solutions from DMRG and imaginary-time evolution (ITE), both with similar energy variance ( $\sigma_H^2 \approx 0.18$ ). The ITE state is initialized with Néel order. As in Eq. (5), the  $y$ -axis indicates each state's contribution to the energy variance. (c) A histogram showing the probability of sampling a local energy in a certain range.

where  $\epsilon_{\max} > 0$  is some specified maximum local deviation. We replace  $\epsilon$  by  $f(\epsilon)$  for estimating the variance. This transformation of the data pushes in the long tails of the local energy distribution to  $\pm\epsilon_{\max}$ , while leaving samples with smaller deviations untouched.

As one might expect, this transformation produces significantly biased variances; see Figure 4(a). We call this the cutoff bias,  $\Delta_c$ . However, in the extrapolation of the energy to zero variance as the bond dimension is in-

creased,  $\Delta_c$  decreases smoothly with the variance, and we find that this bias does not interfere with extrapolation. In order to extrapolate data, we must have a systematic way of choosing  $\epsilon_{\max}$  at each bond dimensions. Note that given a  $\epsilon_{\max}$ , and a set of samples, we can measure the *cutoff ratio*,  $c$ , the percentage of the local energies where  $f(\epsilon) = \epsilon$ . A good approach for determining  $\epsilon_{\max}$  comes from fixing  $c$ . Then the question is: what is the optimal  $c$ , and how well does this method extrapolate?

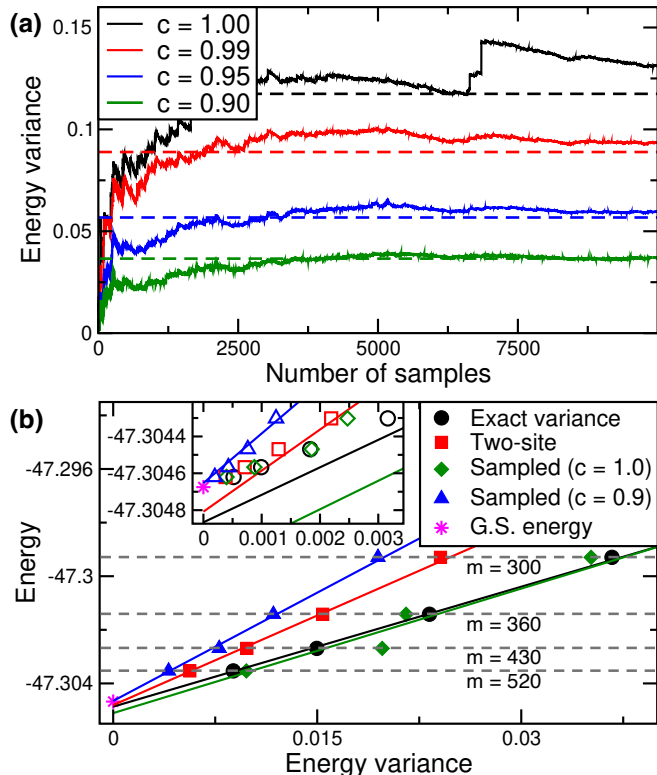


FIG. 4. (a) For the same  $4 \times 4$  torus, the sampled variance of a DMRG state ( $m = 100$ ) at different cutoff ratios, along with exact asymptotic values. The distance from the black dashed line indicated the cutoff bias,  $\Delta_c$ , at each value of  $c$ . (b) For a  $S = 1/2$  Heisenberg model on a  $12 \times 6$  cylinder, extrapolations of ground-state energy using the energy variance, two-site variance, and the sampled variance with and without the bounding extreme samples ( $N_s = 2000$  samples per bond dimension). The unfilled data points on the inset ( $m = 600 - 1300$ ) are not used for extrapolation.

For a variety of models, geometries, and boundary conditions, we have found that setting  $c = 0.90$  provides excellent results; see the SM for the details[9]. As shown in Figure 4(a), as  $c$  decreases the sampling fluctuations drastically decrease; by  $c = 0.9$  the biased variance is determined accurately with a few thousand samples. For this small cluster, we can explicitly compute the asymptotic values [9], as indicated by the dashed lines. In Figure 4(b)

we show extrapolations of the ground-state energy for a  $12 \times 6$  cylindrical Heisenberg cluster, where we compare extrapolations using the exact and two-site variances, as well as from the sampled variance ( $N_s = 2000$  samples) with and without the 90-th percentile cutoff. The higher bond dimension data points on the inset are not used to generate the best-fit lines, but rather to test their accuracy. We find that the  $c = 0.9$  extrapolations offer a significant improvement over the original  $c = 1$  data. Even more, this biased sampling usually extrapolates *better* than the energy variance calculated exactly without sampling. It appears that the fat tails of the variance distribution interfere with extrapolation, even when there is no sampling error. Of course, due to the stochastic nature of sampling, another batch of 2000 samples may do better or worse than this particular batch. Still, over many batches, sampling usually yields energy errors that are generally equal to or quite-often smaller than those from other methods. See the SM for a more details on the performance checks for this extrapolation technique and how it compares to two-site variance extrapolations [9].

*Summary*—We have found that high-energy tails are a universal feature of the energy spectra of MPS approximate ground states. We have argued that this energy structure is an inevitable consequence of the the compression of the ground state into a tensor network, although it would be useful to make this argument more mathematically precise. There are important implications to this unexpected result. For instance, when comparing a DMRG result to a result from another numerical approach, e.g., quantum Monte Carlo, the energy variance of the DMRG state will be significantly larger if the two results have similar errors. An even more significant consequence are large fluctuations in sampling-based approaches. The distribution of sampled local energies have fat tails, impeding the accurate determination of the energy variance. Similar large fluctuations may appear in other approaches, such as MPS-based variational Monte Carlo. However, in the case of the energy variance of DMRG wavefunctions, we found that a biased variance estimator made from bounding the fluctuations can be used to produce excellent extrapolations of the ground state energy at low cost. Importantly, the sampled variance can be computed even in the context of single-site DMRG, in the presence of long range interactions, and without careful design of the sweeping procedure, making it a powerful new tool for DMRG calculations.

*Acknowledgements*—This work was supported by the National Science Foundation under DMR-2110041, as well as by the Eddleman Quantum Institute. We would also like to thank Shengtao Jiang, Miles Stoudenmire, Uli Schollwöck, and Antoine Georges for insightful conversations.

- 
- [1] F. Becca and S. Sorella, *Quantum Monte Carlo Approaches for Correlated Systems* (Cambridge University Press, 2017).
- [2] T. Shi, E. Demler, and J. I. Cirac, *Ann. Phys.* **390**, 245 (2018).
- [3] S. R. White, *Phys. Rev. Lett.* **69**, 2863 (1992).
- [4] U. Schollwöck, *Ann. Phys.* **326**, 96 (2011).
- [5] E. Stoudenmire and S. R. White, *Annu. Rev. Condens. Matter Phys.* **3**, 111–128 (2012).
- [6] S. R. White and D. J. Scalapino, *Phys. Rev. B* **79**, 220504 (2009).
- [7] S. Depenbrock, I. P. McCulloch, and U. Schollwöck, *Phys. Rev. Lett.* **109**, 067201 (2012).
- [8] D. A. H. S. Yan and S. R. White, *Science* **332**, 1173 (2011).
- [9] See Supplemental Material at URL-will-be-inserted-by-publisher for description of lattice models, details about alternative sampling setups, analysis of energy spectra of larger systems, and performance checks of our new extrapolation method on a variety of systems.
- [10] D. Wu, R. Rossi, F. Vicentini, N. Astrakhantsev, F. Becca, X. Cao, J. Carrasquilla, F. Ferrari, A. Georges, M. Hibat-Allah, M. Imada, A. M. Läuchli, G. Mazzola, A. Mezzacapo, A. Millis, J. R. Moreno, T. Neupert, Y. Nomura, J. Nys, O. Parcollet, R. Pohle, I. Romero, M. Schmid, J. M. Silvester, S. Sorella, L. F. Tocchio, L. Wang, S. R. White, A. Wietek, Q. Yang, Y. Yang, S. Zhang, and G. Carleo, Variational benchmarks for quantum many-body problems (2023), arXiv:2302.04919 [quant-ph].
- [11] J. P. F. LeBlanc, A. E. Antipov, F. Becca, I. W. Bulik, G. K.-L. Chan, C.-M. Chung, Y. Deng, M. Ferrero, T. M. Henderson, C. A. Jiménez-Hoyos, E. Kozik, X.-W. Liu, A. J. Millis, N. V. Prokof'ev, M. Qin, G. E. Scuseria, H. Shi, B. V. Svistunov, L. F. Tocchio, I. S. Tupitsyn, S. R. White, S. Zhang, B.-X. Zheng, Z. Zhu, and E. Gull (Simons Collaboration on the Many-Electron Problem), *Phys. Rev. X* **5**, 041041 (2015).
- [12] G. Ehlers, S. R. White, and R. M. Noack, *Phys. Rev. B* **95**, 125125 (2017).
- [13] S. R. White, *Phys. Rev. B* **72**, 180403 (2005).
- [14] C. Hubig, I. P. McCulloch, U. Schollwöck, and F. A. Wolf, *Phys. Rev. B* **91**, 155115 (2015).
- [15] C. Hubig, J. Haegeman, and U. Schollwöck, *Phys. Rev. B* **97**, 045125 (2018).
- [16] E. M. Stoudenmire and S. R. White, *New J. Phys.* **12**, 055026 (2010).
- [17] A. J. Ferris and G. Vidal, *Phys. Rev. B* **85**, 165146 (2012).
- [18] A. W. Sandvik and G. Vidal, *Phys. Rev. Lett.* **99**, 220602 (2007).
- [19] S. Wouters, B. Verstichel, D. Van Neck, and G. K.-L. Chan, Projector quantum monte carlo with matrix product states, *Phys. Rev. B* **90**, 045104 (2014).

# Supplementary materials: Unusual energy spectra of matrix product states

J. Maxwell Silvester<sup>1</sup>, Giuseppe Carleo<sup>2</sup>, and Steven R. White<sup>1</sup>

<sup>1</sup>*Department of Physics and Astronomy, University of California, Irvine, California 92667, USA and*

<sup>2</sup>*Institute of Physics, École Polytechnique Fédérale de Lausanne (EPFL), CH-1015 Lausanne, Switzerland*

(Dated: August 27, 2024)

## A. Description of lattice models

### 1. $S = 1/2$ Heisenberg model

The  $S = 1/2$  Heisenberg model is a nearest-neighbor quantum spin model, useful in the study of a broad range of magnetic phenomena, including antiferromagnetism, ferromagnetism, and spin liquids. The model is described by the Hamiltonian

$$H = J \sum_{\langle i,j \rangle} \vec{S}_i \cdot \vec{S}_j, \quad (1)$$

where the sum ranges over nearest-neighbor pairs. We set  $J = 1$  throughout, corresponding to antiferromagnetic coupling, considering both square and triangular lattices. In the main text we present results for  $4 \times 4$  square lattice clusters with various boundary conditions. For the study of larger clusters below, we also perform calculations for a  $12 \times 6$  square-lattice cylinder. For the triangular lattice, the orientation matters when considering periodic boundary conditions. In our calculations, the lattice is oriented so that when we impose cylindrical boundary conditions, a third of nearest-neighbor bonds are parallel to the periodic direction, with no bonds parallel to the open direction. To avoid frustration, we require a multiple of three sites along this periodic direction, choosing a  $6 \times 6$  triangular lattice cylinder below.

### 2. $J_1$ - $J_2$ model

The  $J_1$ - $J_2$  generalizes the Heisenberg model on a square lattice to include next-nearest-neighbor interactions, with Hamiltonian

$$H = J_1 \sum_{\langle i,j \rangle} \sigma_i \sigma_j + J_2 \sum_{\langle\langle i,j \rangle\rangle} \sigma_i \sigma_j, \quad (2)$$

where the first and second sums over over nearest- and next-nearest-neighbors, respectively. In this work, we set  $J_1 = 1$ , setting the energy scale, and set  $J_2 = 0.2$ . Below we present results for an  $8 \times 8$  open cluster.

### 3. Hubbard model

The Hubbard Hamiltonian is

$$H = -t \sum_{\langle i,j \rangle, s} (c_{i,s}^\dagger c_{j,s} + c_{j,s}^\dagger c_{i,s}) + U \sum_i n_{i\uparrow} n_{i\downarrow}, \quad (3)$$

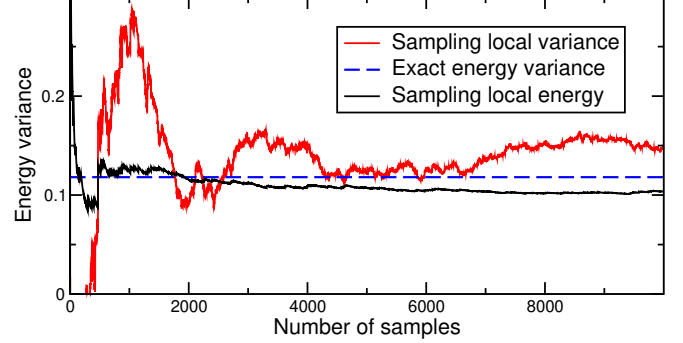


FIG. 1. Running average of the sampled energy variance of a DMRG wavefunction with bond dimension  $m = 100$ , for the  $4 \times 4$  Heisenberg torus. The black curve uses sampled local energies (squared), whereas the red curve uses sampled local variances. The blue dashed line shows the exact energy variance of the state.

where  $c_{i,s}^\dagger$  and  $c_{i,s}$  are the creation and annihilation operators for an electron on site  $i$  with spin  $s$ , and  $n_{i,s} = c_{i,s}^\dagger c_{i,s}$ . The sum in the first term is over nearest-neighbor pairs  $\langle i,j \rangle$  and spins  $s \in \{\uparrow, \downarrow\}$ . We set  $t = 1$  and  $U = 6$  below. We consider only square lattices at half-filling, with an average of one particle per site, focusing on a  $8 \times 4$  cylinder.

## B. Biased vs unbiased sampling

To form an unbiased approximation of the energy variance we can sample the *local variance*,

$$\sigma_s^L = \frac{\langle s | (\hat{H} - E)^2 | \psi \rangle}{\langle s | \psi \rangle}. \quad (4)$$

Just as with the local energies, the local variances are only defined on the wavefunction's support. The energy variance is

$$\sigma_H^2 = \sum_{|s\rangle \in \mathcal{B}} \langle \psi | s \rangle \langle s | (\hat{H} - E)^2 | \psi \rangle. \quad (5)$$

Note that any state that is not in the support necessarily contributes zero to this sum, since its overlap with the wavefunction is exactly zero, by definition. We can therefore replace the sum over all basis elements in Eq. (5) with a sum restricted to the support to get

$$\sigma_H^2 = \sum_{|s\rangle \in \mathcal{S}} P_s \sigma_s^L, \quad (6)$$

where  $P_s = |\langle \psi | s \rangle|^2$ . While this sampling is unbiased, as shown in figure Fig. 1, the results are much noisier than using the biased local energy sampling. Moreover, local variance samples are about a factor of  $w$  more expensive than local energy samples, where  $w$  is the bond dimension of the MPO.

Another approach to eliminating the bias, which works for spin systems, is to sample in a different basis than used for the MPS calculation, for example, sampling spins with measurements in the  $x$  direction instead of the usual  $z$  direction. This eliminates product states with exactly zero weight. However, while this technically eliminates the local energy bias, in practice it only hides it in product states with extremely small probabilities but which contribute a finite amount to the variance. For a spin-1/2 system, this rotated-basis sampling is about a factor of four more expensive than the  $z$ -basis sampling, so again, the naive approach is simpler and cheaper.

### C. Results for larger systems

For larger systems, exact diagonalization or exact ITE without truncation quickly become infeasible as the system size increases. To confirm that the unusual energy structure of MPS wavefunctions holds generically over a broad range of models, boundary conditions and geometries, we require another approach. Here we show that the energy variance helps us to indirectly—yet reliably—measure the extent of high-energy contributions to an approximate ground state. First, note that the energy variance can be rewritten as

$$\begin{aligned} \sigma_H^2 &= \langle \psi | (\hat{H} - E)^2 | \psi \rangle = \sum_{|n\rangle} \langle \psi | n \rangle \langle n | (\hat{H} - E)^2 | \psi \rangle \\ &= c_0^2 (E - E_0)^2 + \sum_{n \neq 0} c_n^2 (E - E_n)^2, \end{aligned} \quad (7)$$

where  $|n\rangle$  are again the energy eigenstates. For a well-converged ITE state, we know that the sum over excited states on the right-hand side of Eq. 7 will only have non-negligible contributions from eigenstates with energy near  $E_1$ ; the coefficients  $c_n$  will be exponentially small if  $E_n \gg E_1$ . Therefore, for ITE states we may approximate the energy variance by replacing  $E_n$  with  $E_1$  in Eq. 7, reaching

$$\begin{aligned} \sigma_H^2 &\approx c_0^2 (E - E_0)^2 + \sum_{n \neq 0} c_n^2 (E - E_1)^2 \\ &= c_0^2 (E - E_0)^2 + (1 - c_0^2) (E - E_1)^2 = \tilde{v}. \end{aligned} \quad (8)$$

In Fig. 2(a), we show, again for the same  $4 \times 4$  Heisenberg torus studied in the main text, how  $v_0 = c_0^2 (E - E_0)^2$  and  $v_1 = (1 - c_0^2) (E - E_1)^2$  contribute to  $\tilde{v}$  as the energy error decreases (by increasing the bond dimension for the DMRG state and increasing imaginary-time for the ITE state). Note that  $v_0$  is an exact term contributing to the

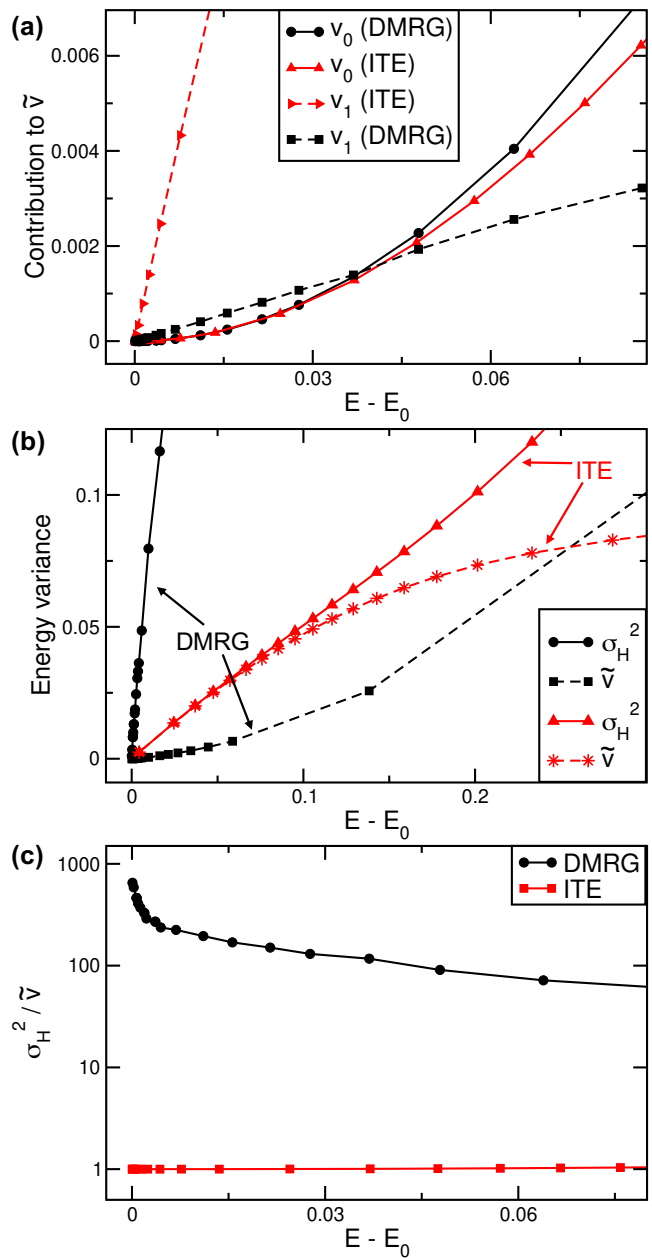


FIG. 2. (a) Components of the approximated energy variance,  $\tilde{v}$ , versus the energy error of the DMRG and ITE states, for the  $4 \times 4$  Heisenberg torus. For the same system, (b) shows the exact versus approximated energy variance and (c) shows the ratio  $\sigma_H^2 / \tilde{v}$ .

variance, while  $v_1$  contains all of the approximations that allows  $\tilde{v} = v_0 + v_1$  to deviate from  $\sigma_H^2$ .

While we expect that  $\tilde{v}$  gives a good estimate of the variance for the ITE state, we do *not* expect this to be the case for the DMRG state; this is because our assumption about the exponential fall-off of the coefficients  $c_n^2$  is not valid in this latter case. In Fig. 2(b) we compare  $\tilde{v}$  to the exact variance for both the DMRG and ITE states. As the energy error decreases, the two values match more



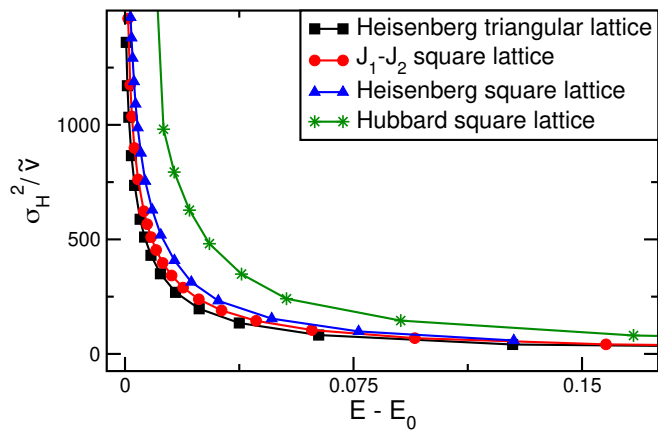


FIG. 3. The ratio  $\sigma_H^2/\tilde{v}$  as DMRG states converge, demonstrating similar high-energy contributions to approximate ground states of larger systems: a  $12 \times 6$  Heisenberg square lattice with cylindrical boundary (blue); a  $6 \times 6$  Heisenberg triangular lattice with cylindrical boundary (black); an  $8 \times 8$   $J_1$ - $J_2$  square lattice with open boundary (red); and an  $8 \times 4$  Hubbard square lattice with cylindrical boundary (green). In all cases,  $\tilde{v}$  is computed by finding highly-converged estimates of the ground and first-excited states via DMRG.

and more closely for ITE state. However,  $\tilde{v}$  severely underestimates the variance for the DMRG state, even at small energy errors.

The ratio  $\sigma_H^2/\tilde{v}$  therefore offers us important information about the energy spectrum. If the ratio is near unity, then the residue is dominated by low-lying excited states; alternatively, if  $\sigma_H^2/\tilde{v} \gg 1$ , then there are significant high-energy contributions to the residue. As shown in Fig. 2(c), the ratio approaches unity as the ITE state converges, while for the DMRG state the ratio *increases* with decreasing energy error. This result for the DMRG state is a consequence of the fact that average energy of the residue increases with increasing bond dimension, as explored in the main text; the increasing energy of the residue makes the assumption about the coefficients  $c_n^2$  less accurate as the bond dimension increases and the approximation in Eq 8 grows correspondingly worse.

In order to calculate  $\sigma_H^2/\tilde{v} = 1$  we require four quantities: the energy of the wavefunction (which comes for free during a DMRG sweep), the overlap of the wavefunction with the exact ground state, and the energies of both the ground- and first excited-state. For larger systems, we cannot compute  $c_0$ ,  $E_0$  and  $E_1$  via exact diagonalization, as we did for the small  $4 \times 4$  cluster above. Instead, we rely on highly converged DMRG results ( $m \approx 10000$ ) to estimate the ground state and first excited state. Results from such an analysis are shown in Fig. 3, for a variety of models. We see that in all cases the ratio is growing as the wavefunctions converge, confirming that these MPS solutions have similar strange energy structure to the smaller clusters explored in the main text.

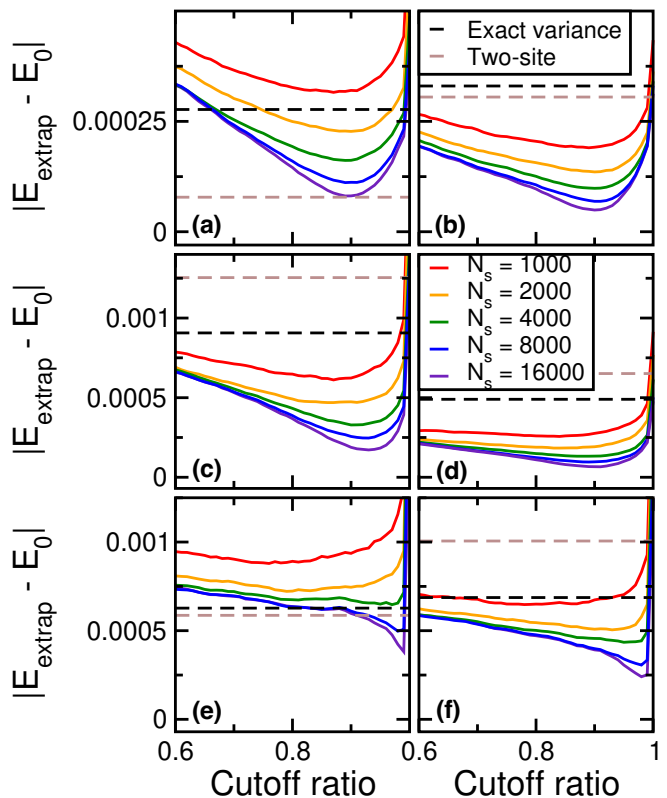


FIG. 4. Optimizing the cutoff ratio for biased variance extrapolations. At each value of the cutoff ratio and the number of samples,  $N_s$ , 1000 sampling-based extrapolations are performed and the average energy errors are plotted as solid lines. Exact and two-site variance extrapolations from the same sweeps are shown as dashed lines. (a) - (b) Heisenberg model on a  $12 \times 6$  square lattice with cylindrical boundary conditions. The maximum bond dimensions of the last sweeps are  $m = 350$  and  $m = 450$ , respectively. (c) - (d) Heisenberg model on a  $6 \times 6$  triangular lattice with cylindrical boundary conditions;  $m = 1000$  and  $m = 1400$ , respectively. (e) - (f)  $8 \times 4$  Hubbard cylinder;  $m = 1400$  and  $m = 1700$ .

#### D. Computing the cutoff bias

In the continuum limit, we define the density of states,  $P(E_L - E)$ , centered around zero and normalized so that

$$\int_{-\infty}^{+\infty} P(E_L - E) dE_L = 1. \quad (9)$$

Recall that the local energies and therefore  $P(E_L - E)$  are only defined over the support of the wavefunction. With the sampling bias in mind, we may write

$$\sigma_H^2 - \Delta_s = \int_{-\infty}^{+\infty} P(\epsilon)\epsilon^2 d\epsilon, \quad (10)$$

where we have changed variables  $E_L - E \rightarrow \epsilon$ . Next, for a given cutoff ratio,  $c$ , we may find the corresponding

cutoff energy,  $\epsilon_c > 0$ , which satisfies

$$c = \int_{-\epsilon_c}^{+\epsilon_c} P(\epsilon) d\epsilon. \quad (11)$$

Note that  $\epsilon_c$  is distinguished slightly from  $\epsilon_{\max}$  used in the main text, since the latter is not necessarily unique. Specifically, there may be a finite gap between two adjacent local energy values; then, any cutoff energy in this gap will yield the same cutoff ratio. On the other hand, there will be exactly one value of  $\epsilon_c$  satisfying Eq. 11. The bias is then

$$\Delta_c = \int_{-\infty}^{-\epsilon_c} P(\epsilon)(\epsilon + \epsilon_c)^2 d\epsilon + \int_{+\epsilon_c}^{+\infty} P(\epsilon)(\epsilon - \epsilon_c)^2 d\epsilon. \quad (12)$$

For a finite system, we rewrite the integrals as sums by introducing the set  $\mathcal{C} \subseteq \mathcal{S}$  of basis states in the support that are cut off because of their extreme local energies. Then, the cutoff ratio is

$$c = \sum_{s \notin \mathcal{C}} P_s \quad (13)$$

and the cutoff bias is

$$\Delta_c = \sum_{s \in \mathcal{C}} P_s (\epsilon_c - |\epsilon|)^2. \quad (14)$$

For a small enough cluster, we can compute the local energies of each basis state and therefore determine the set,  $\mathcal{C}$ , of cutoff states needed to obtain a specified ratio. Of course, for these finite systems, the cutoff ratio can only take on certain discrete values, so there will be some lack of precision in achieving a cutoff ratio of exactly  $c = 0.90$ . However, this error vanishes quickly as the system size increases. For example, for the small  $4 \times 4$  Heisenberg torus that we explore frequently in the main text, a DMRG solution with  $\sigma_H^2 = 0.1175$  and  $m = 100$ , has about 12868 states in the support. This number may fluctuate slightly depending on the “warm up” sweeps used at smaller bond dimension. To approximate a 10% cutoff, we bound the  $|\mathcal{C}| = 4774$  most extreme states and obtain a cutoff ratio of  $c = 0.9000100$  and cutoff energy of  $\epsilon_c = 0.4824$ . The cutoff bias is then found to be  $\Delta_c = 0.0809$ , using Eq. (14).

## E. Extrapolation and optimizing the cutoff ratio

When performing energy extrapolations throughout this work, we use four consecutive data points from running DMRG at increasing bond dimension to create a weighted linear fit. Since sweeps from higher bond dimension are more accurate, this data should be weighted more heavily than lower bond dimension data. Therefore, we set the error estimate for each data point as the measured variance of that point, i.e. the point  $(x, y)$  is assumed to have an error bar of  $x$ .

For our extrapolations from bounded local energy sampling, we wish to find a value of the cutoff ratio that can be held constant across all bond dimensions, yielding high-quality extrapolations. For this optimization, we switch to larger systems more similar to those which would be of interest in a practical DMRG calculation. Still, the system must still be small enough so that we can compute ground-state energies to near numerical precision, enabling us to judge the accuracy of extrapolations from lower dimension data.

For an extrapolation at some fixed value of  $c$ , the absolute energy error  $|E_{\text{extrap}} - E_0|$  is computed, where  $E_0$  is the exact ground-state energy computed via much higher bond dimension DMRG calculations,  $m \approx 10000$ . We repeat this process, generating a batch of  $N_s$  samples at each bond dimension, and computing an energy error. Finally, we average the results from 1000 such batches. In this way we can compute the average energy error at a particular  $c$ -value and compare the result to the errors obtained from extrapolations using both the exact and two-site energy variance. Results from such an analysis for a variety of models and geometries are shown in Fig. 4. We see that the lowest average energy error from our sampling consistently occurs near  $c = 0.9$ . In some cases, the absolute minimum might be closer to  $c = 0.95$  or higher, such as for the Hubbard model plots. However, in other cases a cutoff ratio greater than 0.9 decreases the accuracy of extrapolations, as in the Heisenberg square lattice plots. In all cases  $c = 0.9$  is close to optimal and performs competitively, or simply better, than the exact or two-site extrapolations. It is interesting to note that the two-site variance seems to yield extremely accurate extrapolations in Fig. 4(a). However, performing just one more sweep at a modestly increased bond dimension, the two-site extrapolations are significantly worse than the average results from sampling with  $c = 0.9$ , as shown in Fig. 4(b). In general it seems that the energy error from the two-site extrapolation is anomalously low in (a).